Influence of Thermal Tempering Processes on Color Stability of Glass-infiltrated Monochrome and Multilayer 5 mol% Yttria Partially Stabilized Zirconia

Keywords

Color Characteristics
CAD-CAM
Color Stability
Glass Infiltration
Thermal Tempering

Authors

Pithiwat Uasuwan *
(DDS, MSc, PhD)

Niwut Juntavee §
(DDS, CAGS, MSD, DScD)

Apa Juntavee ‡
(DDS, CAGS, MPH, PhD)

Address for Correspondence

Niwut Juntavee §

Email: niwutpapa@hotmail.com

* *Division of Biomaterials and Prosthodontics Research, Faculty of Dentistry, Khon Kaen University, Khon Kaen, 40002, Thailand*

§ *Department of Prosthodontics, Faculty of Dentistry, Khon Kaen University, Khon Kaen, 40002, Thailand*

‡ *Division of Pediatric Dentistry, Department of Preventive Dentistry, Faculty of Dentistry, Khon Kaen University, Khon Kaen, 40002, Thailand*

Received: 02.11.2024
Accepted: 10.02.2025

doi: 10.1922/EJPRD_2832Uasuwan12

ABSTRACT

*Introduction: This study investigated the effects of tempering on color stability of glass-infiltrated monochrome (Mo) and multilayer (Mu) 5 mol% yttria-partially stabilized zirconia (5Y-PSZ). Materials and Methods: 180 5Y-PSZ specimens (width-length-thickness = 10-20-2 mm) were prepared from Mo and Mu, comprising cervical (C) and incisal (I) zone, and sintered with traditional versus glass infiltrated technique with different tempering processes through slow (S: 5°C/min), normal (N: 35°C/min), and fast (F: 70°C/min) cooling. CIE-L*a*b*, color difference (ΔE_{diff}), and microstructures were evaluated. ANOVA and Tamhane's comparisons were determined for significant differences ($p<0.05$). Results: Mo closely resembled MuI for L* and a*, but was similar to MuC for b* and ΔE_{diff}. MuC exhibited significantly higher L*, a*, and b*, but lower ΔE_{diff} than MuI. Glass infiltration and fast tempering significantly increased L*, and ΔE_{diff}, whereas decreased a*, and b*. Mu had higher color change than Mo, but both were within an acceptable threshold ($\Delta E_{diff} \leq 5.5$). Conclusions: Glass infiltration and tempering processes altered color, with greater influence on Mu>Mo. Glass infiltration and rapid tempering produced a white-chalky and less chroma due to smaller grain size and t→m transformation. Nevertheless, color alterations were still within acceptable limits, thus considered color stable.*

INTRODUCTION

Ceramics have been utilized for aesthetic dentistry for many years due to their exceptional physical characteristics. As a consequence of the ongoing development of digital technology, several state-of-the-art dental ceramics have been introduced in response to patient needs. One of the appealing ceramics is stabilized zirconia, due to its excellent physical and mechanical properties, dimensional stability, and chemical inertia.[1] Zirconia encompassed three microstructural phases including tetragonal (t-), monoclinic (m-), and cubic (c-) phases. All phases are interchangeable due to the triggered temperature. At the ambient temperature, the m-phase was detectable. Upon heating up to 1,170°C, the m-phase was induced to transform to the t-phase until the temperature reached 2,370°C, and the c-phase appeared and remained unchanged up to the melting point of 2,680°C.[2] As cooling down, all the microstructures turn into the m-phase.

ejprd.org - Published by Dennis Barber Journals. Copyright ©2024 by Dennis Barber Ltd. All rights reserved.

To achieve and stabilize the desired t- and c-phases at room temperature, a yttrium oxide stabilizer (Y_2O_3) was added.[2] The 3 mol% yttrium oxide was first implemented into zirconia as called 3 mol% yttria-stabilized tetragonal polycrystalline (3Y-TZP). This 3Y-TZP presented almost the entire t-phase at the normal temperature. The zirconia microstructure transitions from the t→m phase causing 4–5% expansion as induced by external stimuli such as moisture, stress, and warmth, giving stabilized zirconia an exceptional strength called "transformation toughening", a process that creates compressive stress generated by the volumetric expansion of phases to withstand crack propagation.[1] However, the light scattering on 3Y-TZP, given its opacity, has to be tremendously concerned for monolithic use.

Various techniques have been employed to enhance the light transmission of monolithic zirconia, such as varying the sinter settings, adjusting the quantity and magnitude of alumina, and altering the Y_2O_3 concentration.[3] Adding up to 5 mol% yttrium oxide to monolithic zirconia, called "5 mol% yttria-partially stabilized zirconia (5Y-PSZ)", can develop approximately 50% cubic structures.[3] Because of their larger volume and increased isotropy, these cubic structures improve light transmission through the material by reducing light scattering at the grain boundaries and uniformly radiating incident light across the structure.[3] However, this extremely translucent 5Y-PSZ ceramics presented with a decreased mechanical strength since it had less transformation toughening as a result of the minimal t-phase presented.[4] Monolithic zirconia can be classified into monochrome (Mo) and multilayer (Mu) zirconia. The Mo zirconia represents the single material's color for the entire zirconia block, while the Mu zirconia has a chromatic gradient shift from the cervical to the incisal area mimicking the natural dentition.[5] Previous studies proved that the color gradience between each zone of Mu zirconia was due to the pigment addition.[5] For example, increasing ferric oxide (Fe_2O_3) led to a material loss of translucency.[6] The utilization of increased cerium and bismuth concentrations led to a significant rise in the b* color coordinate.[7] However, certain studies indicated no substantially different translucency[5] and flexure strength[8] across distinctive levels of zirconia. The Mo and Mu 5Y-PSZ are mostly limited to use for single and short-span fixed restoration due to their sacrificed strength, and the translucency was still lesser than that of lithium disilicate glass ceramics.[9] When choosing a material, especially in the realm of aesthetics, color perception is the most important factor to take into account.[10] The amount of light trajectory has been observed to be influenced by the material's grain size and distribution, crystal microstructure, color pigments, and defect pores.[11] The process is when light is reflected off the object, it should seem blueish, and when light passes through it, it should appear orange. It is vital for accurately imitating the natural enamel as an opal appearance.[12,13] As far as the color perceptibility threshold was concerned, it was investigated through the color difference value (ΔE_{diff}). This value could be classified as within the perceptibility threshold (PT, $\Delta E_{diff} \leq 2.6$) and the acceptability threshold (AT, $\Delta E_{diff} \leq 5.5$).[14] The more the color difference value, the more the color distinguishment, and the less the acceptability in color stability.

An endeavor to improve the strength and esthetics of 5Y-PSZ is to invent a suitable silicate glass with a lower modulus to be graded on the outer surfaces of porous zirconia called graded zirconia.[15,16] Such a gradation is expected to reduce the tensile stress intensity at the outer surfaces of restoration[17], where fractures frequently begin, making the structure less prone to fracture. In terms of esthetics, a study showed that the translucency of the infiltrated zirconia was improved relatively to those of conventional core materials; however, it was not as high as that for dental porcelains.[18] On the other hand, another study showed a decreased translucency and increased color difference value than the non-infiltration counterpart.[19] The glass infiltration can be done on intaglio and/or cameo surfaces of restoration. The glass deposition on the external surface also acts as an encapsulation layer that could oppose water absorption, prevent hydrothermal degradation, protect against antagonist attrition, and permit color disparities, eventually leading to esthetics improvement.[15,20] Moreover, the formation of glass on the cementation surface makes acid etching and silanization feasible, enhancing bonding to resin cement.[20] The color of the glass infiltration could be adjusted to match the surrounding structure by incorporating color additives during the process or applying staining after the glass infiltration.[16] This glass infiltration requires a first firing procedure for making more stabilized porous zirconia from the pre-sintered block and a second firing procedure for the glass infiltration into the porous zirconia. Therefore, the fabrication of graded zirconia is time-consuming.

To improve the physical properties of stabilized zirconia, the adjustment of firing parameters was considered a cost-effective strategy. This modification impacted material density, pore reduction, and crystal structure.[21] Firing monolithic zirconia at higher temperatures was known to increase its translucency.[21] Additionally, prolonging the sintering time of 3Y-TZP led to grain growth, significantly improving optical characteristics and triggering the t- to m-phase transition.[10] Rapid thermal tempering of stabilized zirconia has been shown to increase translucency by promoting a bigger grain magnitude[22] and inducing a t→m phase change.[23,24] The impact of altering the thermal tempering process on color characteristics was still insufficient, and controversial results regarding glass infiltration in 5Y-PSZ. Until now, there was no commercial product for glass infiltration with suitable firing parameters to optimize the physical characteristics of dental zirconia. The invention of glass composition has been challenging for researchers and requires further experimental tests. In this study, we developed glass infiltration powder along with different sintering techniques and examined their impacts on the color parameters of Mo and Mu 5Y-PSZ. The tested null hypothesis of this investigation posited as 1) the color parameters of 5Y-PSZ would not be influenced by the

ejprd.org - Published by Dennis Barber Journals. Copyright ©2025 by Dennis Barber Ltd. All rights reserved.

different sintering techniques based on glass infiltration, 2) the color parameters of 5Y-PSZ would not be influenced by the different thermal tempering processes, 3) the color parameters of 5Y-PSZ would not be influenced by the different material types, and 4) the color parameters of 5Y-PSZ would not be influenced by their relations.

MATERIALS AND METHODS

The sample size for this experimental investigation was derived from the statistical data performed by Sailer and colleagues' publication in 200725 using software G*Power version 3.1 (Heinrich Heine University, Dusseldorf, Germany) at 90% power of test with α error of 0.05 as shown in Equation 1.

$$\text{N per group} = \frac{(Z\alpha_{/2}+Z\beta)^2\,(s_1{}^2+s_2{}^2)}{(\mu_1-\mu_2)^2} \qquad \text{Equation (1)}$$

Which: Z_β = standard normal deviation = 1.28 (β error = 0.1), Z_α = standard normal deviation = 1.96 (α error = 0.05), s = standard deviation (s_1 = 2.3, s_2 = 1.5), and μ_1 - μ_2 = mean difference between tested group = 0.8. The calculated sample size was employed 15 specimens per group.

ZIRCONIA SPECIMENS PREPARATION

One hundred eighty (180) tested specimens were prepared from multilayer (Mu: Cercon xt ML, Dentsply Sirona, Charlotte, NC, USA), and multilayer (Mo: Cercon xt, Dentsply Sirona) 5Y-PSZ block. The chemical compositions of 5Y-PSZ were ZrO_2+HfO_2+Y_2O_3 ≥99%, Y_2O_3 9%, HfO_2 <3%, and Al_2O_3,+SiO_2 <1%. The Mu and Mo 5Y-PSZ samples were cut with a diamond-coated wheel at a speed of 700 rounds per minute (rpm) by a precision machine (Mecatome-T180, PRESI, Eybens, France) by cooling with water. Waterproof SiC abrasive sheets up to no. 2000 were used to grind the 5Y-PSZ samples in a wet condition with water using a grinding apparatus (Ecomet-3, Beuhler, Lake Bluff, IL, USA) at 40 rpm speed. After that, specimens were polished using suspension with fine diamond particles mounted to a polishing apparatus (Ecomet-3, Beuhler) at 80 rpm speed. The specimens were ultrasonically cleaned in distilled water using an ultrasonic cleansing machine (Vitasonic-II, Vita Zahnfabrik, Bad Säckingen, Germany) for ten minutes and lastly dried at room temperature for an hour. To attain a specified dimension (width, length, thick = 10, 20, 2 mm), the samples were originally prepared at an enlarged slab (width, length, thick = 12.5, 25, 2.5 mm) for compensation of sintering shrinkage *(Figure 1A)*. Once sintering, the samples accomplished the final sizes and were measured with digital vernier calipers (Mitutoyo, Kanagawa, Japan).

PREPARING GLASS INFILTRATION POWDER

The glass powder (In-house glass, Division of Biomaterials, KKU, Khon Kaen, Thailand) was prepared as its elemental composition was SiO_2 66.8%, Al_2O_3 12%, Na_2O 10%, K_2O 7.9%, CaO 3%, and Fe+Ti+Mg 0.3%. These oxides were ground and uniformly mixed in a crucible. Finally, a serial sieving procedure was done in a chamber to achieve a fine powder size under 150 mesh. The glass infiltration powder was stored in a sealed glass bottle before use *(Figure 1B)*.

ZIRCONIA SINTERING PROCEDURE

The Mo and Mu 5Y-PSZ specimens were randomly distributed to be sintered according to two sintering techniques: glass infiltration (G), and traditional (T) sintering, and different thermal tempering strategies through three cooling modes: fast cooling (F, 70°C/min), normal cooling (N, 35°C/min), and slow cooling (S, 5°C/min) (n = 15/group). For G-sintering groups, the 5Y-PSZ specimens were initially sintered to form the porous zirconia by heating to 880°C at a speed of 22°C/min, then 11°C/min to reach a maximum temperature of 1350°C and held for 1 hour, followed by cooling down per three tempering strategies (S, N, and F). After reaching room temperature, the in-house glass was mixed with distilled water and then smeared on the zirconia surface of the samples with a soft camel brush. The 100-micron thick glass was applied on one external surface side and was controlled by a custom acrylic template *(Figure 1C)*. A final sintering was done by heating to 880°C at a speed of 22°C/min, then 11°C/min to reach a maximum temperature of 1500°C and held for 2 hours. After that, cooling down to normal temperature using the assigned tempering speeds. (S, N, and F). For T-sintering groups, the 5Y-PSZ specimens were sintered by heating to 880°C at a speed of 22°C/min, then 11°C/min to reach a maximum temperature of 1500°C and held for 2 hours. After that, cooling down to normal temperature using the assigned tempering modes. (S, N, and F). The aforementioned sintering procedure was performed in a high-temperature furnace (inFireHTC, Dentsply Sirona). The sintered specimens were cleaned by a high-frequency ultrasonic device (Vitasonic-II, Vita Zahnfabrik) for 10 minutes, and were air-dried at normal room temperature before testing *(Figure 1D)*.

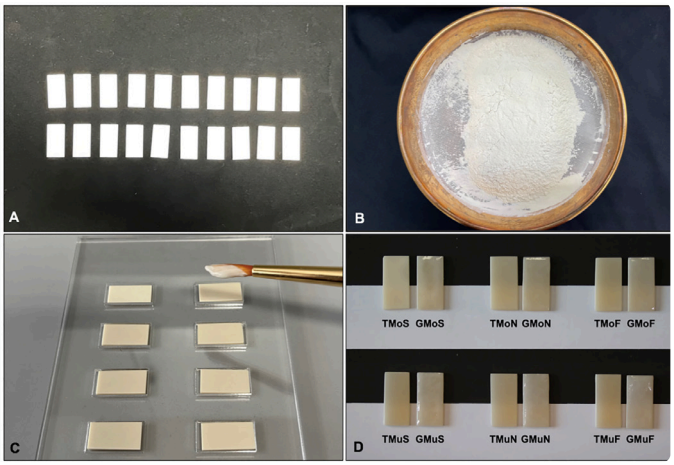

Figure 1: The 5Y-PSZ specimens after sectioning (A), and invented glass infiltration powder (B), were prepared. The glass mixture was applied on first-sintered porous zirconia with an acrylic template for thickness control (C). The traditional (T) and glass infiltrated (G) monochrome (Mo), multilayer (Mu) 5Y-PSZ specimens were sintered upon slow (S), normal (N), and fast (F) cooling strategy (D).

ejprd.org - Published by Dennis Barber Journals. Copyright ©2025 by Dennis Barber Ltd. All rights reserved.

DETERMINATION COLOR PARAMETERS

The color characteristics of traditional and glass-infiltrated Mo and Mu 5Y-PSZ with different sintering strategies were achieved using a laboratory spectrophotometer (ColorQuest XE, Hunter, Reston, VA, USA). The instrument was calibrated with a standard white tile before starting the measurements. A transparent acrylic template was employed to maintain the position of the specimen during the optical parameter measurement. The cervical (C) and incisal (I) portions of Mu 5Y-PSZ were measured independently. Three measuring points were taken at the midpoint of the left, central, and right sides for each portion of the specimen. The testing apparatus was adjusted to D65 illuminant, 10% observing angle, 100% UV, and 380-780 nm of standard wavelength. The color determinations were blindly performed on each specimen in CIELab (Commission Internationale de I'Eclairage) by one well-qualified examiner. The L*, a*, and b* color parameters were attained from the lightness (L^*_w), the red-green coordinate (a^*_w), and the yellow-blue (b^*_w) coordinate of samples, respectively, on standard white (W) background.[19,21] Then, the color coordinates of the VITA classical (Vita Zahnfabrik) shade A2 on a white background (L_{A2}= 65.61, a_{A2} = -0.50, b_{A2}= 5.54) were measured and used for determination color difference (ΔE_{diff}) according to Equation (2).[11]

$$\Delta E_{diff} = \sqrt{(L^*_W - L^*_{A2})^2 + (a^*_W - a^*_{A2})^2 + (b^*_W - b^*_{A2})^2}$$

Equation (2)

EXAMINING THE MICROSTRUCTURE AND CHEMICAL COMPOSITION

Three samples of each group were unintentionally chosen for electroplating with gold for three minutes at 10 mA of a current and a vacuum of 130 mTorr and then were dried in a desiccator cabinet. For the Mu 5Y-PSZ, the incisal (I) and cervical (C) zones were evaluated separately. The scanning electron microscope (SEM, Hitachi-SU3800, Osaka, Japan) coupled with an energy dispersive analysis of X-ray (EDAX) was used to evaluate the microstructure and chemical components. The Image-J software (U.S. National Institutes of Health, Bethesda, MD, USA) was used for assessing the grain size. The cross-sectional micrograph was also performed to characterize of residual glass and infiltration zone.

DETERMINING THE PHASE PROPORTION

The relative proportions of zirconia crystal phases were measured using an X-ray diffractometer (MiniFlex 2, Rigaku, Tokyo, Japan). The specimens were probed with copper k-alpha (Cu Kα) ray at intervals of two seconds, with the angles of diffraction (2θ) ranging from 20 - 80 degrees (°) at 0.02° stepwise. The phases of zirconia were appraised by cross-reference with the Joint Committee of Powder Diffraction Standards database file (PDF). The analysis of the t-, m-, and c-phase proportion was performed by Rietveld refinements with powder diffraction analysis software (Match! software version 3.15, Bonn, Germany) related to the intensity of the peak. The peaks for the m-, t-, and c-phases were identified in the PDFs No. 37–1484, 49–1642, and 42–1164, respectively. The m-phase proportion (X_m) was calculated using Equation 3.[24] The integrated intensity of the m-, t-, and c-phases (I_m, I_t, and I_c) were estimated by matching the complementary peaks with a pseudo-Voigt distribution and considering the area beneath the curves. A correction factor of 1.311 was established from a non-linear adjustment curve of the integrated intensity fractions versus volume fraction to take the impact of yttria doping on the lattice parameters into consideration. The quantity of t-phase (Xt) and c-phase (Xc) was computed from Equations 4 and 5.[24]

$$X_m = \frac{1.311[I_m(111)+I_m(11-1)]}{1.311[I_m(111)+I_m(11-1)]+I_t(111)}$$

Equation (3)

$$X_C = 1 - \frac{I_t(004)+I_t(220)}{I_t(004)+I_t(220)+I_c(400)}$$

Equation (4)

$$X_t = 1 - (X_m + X_c)$$

Equation (5)

STATISTICS ANALYSIS

The data were accomplished for the normality test with the Shapiro-Wilk test, and the homoscedasticity test with Levene's test using IBM SPSS V-28 statistics software (SPSS, Chicago, IL, USA). As the data revealed normal distribution and exhibited homoscedasticity (p>0.05), the three-way analysis of variance (ANOVA) along with Tamhane-T2 Post hoc multiple comparisons were implemented to detect substantial variations in the optical characteristics between Mu and Mo 5Y-PSZ under the influence of several sintering techniques and various tempering protocols. A statistically significant difference was judged at p<0.05. Furthermore, descriptive statistics were employed to evaluate the optical properties, grain size, elemental composition, and relative phases of zirconia.

RESULTS

The mean of L^*_w, a^*_w, b^*_w, and color difference (ΔE_{diff}), together with their standard deviation (SD) of experimental groups were presented *(Figure 2 and Table 1)*. The type of zirconia materials, sintering strategies, thermal tempering processes, and their interactions significantly affected all color characteristic values (p<0.05), except for the interaction of material and sintering to a*, and the interaction of the three factors to L*, as revealed by the result of three-way ANOVA *(Table 2)*. Post hoc Tamhane-T2 results for each optical parameter were presented in Table 3. Regarding the Mu 5Y-PSZ materials, MuC presented significantly higher L*, a*, and b*, but lower ΔE_{diff} than MuI (p<0.05). The Mo demonstrated closer L*, and a* values to MuI; however, closer b* and ΔE_{diff} values to MuC. Rapid thermal tempering process and/or infiltration with the glass significantly increased L* and ΔE_{diff} whereas significantly decreased a*, and b* values (p<0.05) as indicated in Post hoc multiple comparisons *(Table 3)*. The application of glass and

ejprd.org - Published by Dennis Barber Journals. Copyright ©2025 by Dennis Barber Ltd. All rights reserved.

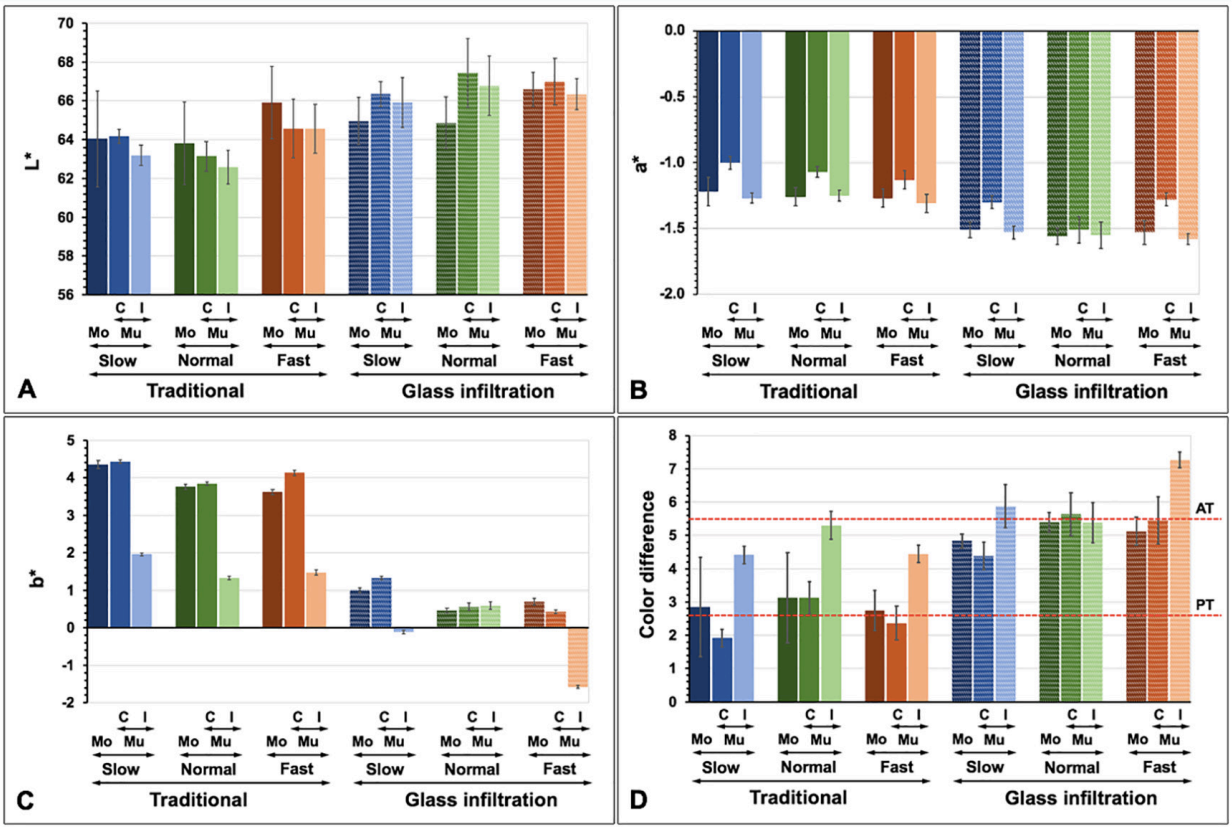

Figure 2: The optical parameters including L* (A), a* (B), b* (C), and color difference (D) with a perceptible threshold (PT) and acceptable threshold (AT) of traditional and glass infiltrated monochrome (Mo), multilayer (Mu, C: cervical; I: incisal) 5Y-PSZ upon slow, normal, and fast thermal tempering processes were shown.

increasing rate of thermal tempering produced a more white, less red-yellow, and more green-blue appearance in 5Y-PSZ *(Figure 3)*. Concerning the color difference (ΔE_{diff}) for shade matching to A2 VITA classical shade, the MuCS and MuCF were considered within a PT ($\Delta E_{diff} \leq 2.6$), whereas the remaining groups except GMuIS, GMuCN, and GMuIF were considered within an AT ($\Delta E_{diff} \leq 5.5$). However, the mean ΔE_{diff} value of the different types of materials (Mo, MuC, and MuI), sintering techniques (T, and G), or different thermal tempering (S, N, and F) was within the AT.

The microscopic structures of Mo and Mu 5Y-TZP were depicted from the SEM and EDS. The zirconia crystals were classified into four groups based on their grain size: ultrafine (≤0.4 µm), fine (0.4<x≤0.7 µm), medium (0.7<x≤1 µm), and large (>1 µm), and their relative percentage of grain distribution were presented *(Figure 4A and Table 1)*. The average grain size (mean ± SD, µm) of Mo (1.03 ±0.42) was larger than MuC (1.02 ± 0.36) and MuI (1.01 ± 0.44). The larger zirconia grain size was observed in glass-infiltrated sintering (1.18 ± 0.42) compared to traditional sintering (1.02 ± 0.40) of 5Y-PSZ. Moreover, the S-tempering protocol illustrated the biggest grain size, followed by the N- and F-tempering protocols. However, the average grain sizes of Mo 5Y-PSZ and C- and I-halves of Mu 5Y-PSZ were not remarkably different *(Figure 5)*. The relative percentage of the grain size distribution for each type of 5Y-PSZ was influenced by the sintering technique and thermal tempering process *(Figure 4A and Table 1)*. The percentage of large grain sizes was likely to increase while sintering with the glass infiltration technique as well as decelerating the thermal tempering. Regarding the composition analysis by EDS, the traditional 5Y-PSZ presented major elements (%wt) of zirconia (72.2 - 78.3), oxygen (11.1 - 18.0), and yttrium (7.2 - 7.7). The amount of yttrium was equivalent to 5mol% yttrium oxide. While the amount (%wt) of oxygen (32.2 - 55.5), silica (26.5 - 47.1), and alumina (5 - 9.8) were detected as a majority on the residual glass of glass infiltrated 5Y-PSZ *(Figure 4B)*.

The quantity of the zirconia phase was investigated by XRD as demonstrated *(Figure 4C, D, and Table 1)*. The XRD patterns for all experimental groups illustrated the t-phase as the principal phase, trailed by the c- and m-phase. The t-phase was majorly observed at 2θ degree of 30.00º, 34.86º, 73.20º, and 74.20º, the c-phase was shown at 74.70º, as well as the m-phase was detected at 28.00º and 31.20º. All testing groups showed that the percentage (%) of t-phase (47.1 - 52.0) was slightly higher than that of c-phase (41.4 - 47.5). The amount of zirconia phases was concurrent with the zirconia sintering technique and the thermal tempering. It was observed that the m-phase was likely to increase as a result of infiltration sintering with the glass and fast thermal tempering.

The SEM images of traditional 5Y-PSZ, and glass-infiltrated 5Y-PSZ were shown *(Figure 5)*. The F-thermal tempering impeded the formation of zirconia grains, resulting in smaller grains than those generated by S- and N-thermal tempering patterns in both traditional and glass-infiltrated 5Y-PSZ *(Figure 4)*. Concerning the surface morphology of the infiltrated zone of glass-infiltrated 5Y-PSZ, the images revealed that the zirconia grains

ejprd.org - Published by Dennis Barber Journals. Copyright ©2025 by Dennis Barber Ltd. All rights reserved.

Table 1. Mean, standard deviation (SD) of L^*_w, a^*_w, b^*_w, color difference (ΔE_{diff}), relative monoclinic (m-), tetragonal (t-), and cubic (c-) phase content (wt.%), and percentage of ultrafine (u), fine (f), medium (m), and large (l) grain size distribution (%) of traditional (T) and glass infiltrated (G), monochrome (Mo), multilayer [(Mu: cervical (C), incisal (I)] 5Y-PSZ upon slow- (S), normal- (N), and fast- (F) thermal tempering processes.

Group	n				ΔE_{diff}	Phase (wt%)	Grain size (%)
		Mean±SD	Mean±SD	Mean±SD	Mean±SD	m- / t- / c-	U / f / m / l
TMoS	15	64.0±2.5	-1.2±0.1	4.4±0.3	2.8±1.5	4.4 / 49.8 / 45.8	0.0 / 16.4 / 35.8 / 47.8
TMuCS	15	64.2±0.4	-1.0±0.1	4.4±0.3	1.9±0.3	4.9 / 50.1 / 45.0	1.5 / 12.1 / 39.4 / 47.0
TMuIS	15	63.2±0.5	-1.3±0.1	2.0±0.3	4.4±0.3	4.5 / 50.5 / 45.0	0.0 / 18.3 / 35.4 / 46.3
TMoN	15	63.8±2.1	-1.3±0.1	3.8±0.6	3.1±1.4	4.4 / 50.0 / 45.6	1.3 / 21.3 / 29.3 / 48.0
TMuCN	15	63.1±0.8	-1.1±0.1	3.8±0.4	3.1±0.5	5.1 / 49.4 / 45.5	0.0 / 19.7 / 31.6 / 48.7
TMuIN	15	62.6±0.9	-1.3±0.1	1.3±0.3	5.3±0.4	5.2 / 50.3 / 44.5	4.6 / 24.1 / 25.0 / 46.3
TMoF	15	65.9±1.9	-1.3±0.1	3.6±0.5	2.7±0.6	5.0 / 49.3 / 45.7	8.1 / 27.6 / 19.5 / 44.8
TMuCF	15	64.6±1.5	-1.1±0.1	4.1±0.5	2.4±0.5	6.0 / 50.4 / 43.6	0.0 / 29.7 / 30.7 / 39.6
TMuIF	15	64.6±1.2	-1.3±0.1	1.5±0.3	4.4±0.3	5.4 / 50.4 / 44.2	1.4 / 16.7 / 43.1 / 38.9
GMoS	15	65.0±1.2	-1.5±0.1	1.0±0.3	4.8±0.2	5.5 / 49.6 / 44.9	2.3 / 10.2 / 21.6 / 65.9
GMuCS	15	66.4±0.6	-1.3±0.1	1.3±0.3	4.4±0.4	6.4 /4 9.9 / 43.7	4.1 /8.1 / 16.2 / 71.6
GMuIS	15	65.9±1.3	-1.5±0.1	-0.1±0.6	5.9±0.6	6.6 / 52.0 / 41.4	2.4 / 7.1 / 16.7 / 73.8
GMoN	15	64.9±1.3	-1.6±0.1	0.5±0.3	5.4±0.3	5.4 / 47.1 / 47.5	2.3 / 7.9 / 14.6 / 75.3
GMuCN	15	67.4±1.8	-1.5±0.1	0.6±0.3	5.6±0.6	5.2 / 48.8 / 46.0	2.7 / 12.0 / 24.0 / 61.3
GMuIN	15	66.8±1.5	-1.6±0.1	0.6±0.5	5.4±0.6	5.2 / 50.5 / 44.3	0.0 / 14.0 / 5.6 / 60.5
GMoF	15	66.6±0.9	-1.5±0.1	0.7±0.3	5.1±0.4	7.3 / 49.5 / 43.2	0.0 / 10.6 / 27.7 / 61.7
GMuCF	15	67.0±1.2	-1.3±0.1	0.4±0.5	5.4±0.7	5.7 / 47.6 / 46.7	0.0 / 14.0 / 27.9 / 58.1
GMuIF	15	66.3±0.8	-1.6±0.1	-1.6±0.2	7.3±0.2	6.3 / 49.7 / 44.0	3.0 / 13.1 / 19.2 / 64.7

were loosely bonded, and there were gaps between the grains, providing room for silica infiltration. The SEM cross-sectional image along with the EDS line scan of glass infiltrated 5Y-PSZ illustrated the residual glass of ~60-80 µm, the infiltration area of ~52-59 µm, and the innermost dense zirconia grain. The S-thermal tempering seemed to have a lesser infiltration depth and presented thicker residual glass.

DISCUSSION

In this study, we innovated a glass powder for conducting glass infiltration on Mo and Mu 5Y-PSZ while simultaneously varying the sintering technique. Both Mo and Mu 5PSZ specimens were firstly fired to create the porous zirconia, which had the gap and inter-grain hollow, and afterward the invented glass onto the surface. Upon the second firing, the glass then infiltrated into a space between grains of porous zirconia by the capillary force, to completely form the inter-networking between glass and zirconia, along with the optimization of sintering cooling strategies, to achieve the glass infiltrated 5Y-PSZ. Subsequently, the color parameters were measured in comparison between glass infiltrated and traditional (non-infiltration) sintering counterparts. The results revealed significant effects of material type, thermal tempering processes, and sintering strategies, as well as their interactions, on all color parameter values ($p<0.05$), except the interaction of material and glass to a*, and the interaction of three factors to L*. Hence, all tested null hypotheses were rejected, except for the interaction of material and glass to a*, and the interaction of three factors to L*.

Regarding the type of materials, Mo, MuC, and MuI 5Y-PSZ showed significant differences in all parameters. A slight disparity in color additives, as noted in a previous study[5], played a crucial role in color perception. In the non-infiltration groups, Mo tended to appear whiter, indicated by an enlarged L* value compared to Mu. Additionally, MuI appeared darker, with a lessened L* value compared to MuC, consistent with the natural character of a tooth where the incisal part typically displays a black incisal halo and more shadowing than the cervical part. The MuC exhibited higher chroma (higher a* and b*) than MuI, resembling the chromatic properties of a natural tooth that increase from I- to C-zone.[26] The I-zone had lower a* and b*

ejprd.org - Published by Dennis Barber Journals. Copyright ©2025 by Dennis Barber Ltd. All rights reserved.

Table 2. Three-way ANOVA of L^*_w (A), a^*_w (B), b^*_w (C), (D) color difference (ΔE_{diff}) of traditional and glass infiltrated sintering of monochrome and multilayer 5Y-PSZ with different thermal tempering processes.

Source	SS	df	MS	F	p
A. ANOVA of L^*_w upon different factors					
Material	14.846	2	7.423	4.018	0.019
Sintering	341.291	1	341.291	184.733	0.001
Cooling	67.508	2	33.754	18.270	0.001
Material * Sintering	63.268	2	31.634	17.123	0.001
Material * Tempering	19.820	4	4.955	2.682	0.032
Sintering * Tempering	30.754	2	15.377	8.323	0.001
Material * Sintering * Tempering	12.506	4	3.127	1.692	0.152
Error	465.565	252	1.847		
B. ANOVA of a^*_w upon different factors					
Material	2.120	2	1.060	229.248	0.001
Sintering	5.524	1	5.524	1194.897	0.001
Cooling	.170	2	.085	18.382	0.001
Material * Sintering	.006	2	.003	.641	0.528
Material * Tempering	.188	4	.047	10.168	0.001
Sintering * Tempering	.172	2	.086	18.557	0.001
Material * Sintering * Tempering	.167	4	.042	9.028	0.001
Error	1.165	252	.005		
C. ANOVA of b^*_w upon different factors					
Material	189.319	2	94.660	630.380	0.001
Sintering	542.328	1	542.328	3611.603	0.001
Cooling	22.519	2	11.260	74.982	0.001
Material * Sintering	26.494	2	13.247	88.216	0.001
Material * Tempering	11.784	4	2.946	19.619	0.001
Sintering * C Tempering	6.970	2	3.485	23.208	0.001
Material * Sintering * Tempering	15.271	4	3.818	25.423	0.001
Error	37.841	252	.150		
D. ANOVA of ΔE_{diff} upon different factors					
Material	143.491	2	71.745	172.209	0.001
Tempering	303.308	1	303.308	728.025	0.001
Cooling	19.913	2	9.956	23.898	0.001
Material * Sintering	17.328	2	8.664	20.796	0.001
Material * Tempering	14.470	4	3.618	8.683	0.001
Sintering * Tempering	15.437	2	7.719	18.527	0.001
Material * Sintering * Tempering	15.179	4	3.795	9.109	0.001
Error	104.988	252	.417		

Abbreviations: SS: sum of squares, df: degree of freedom, MS: mean square, F: F-ratio.

ejprd.org - Published by Dennis Barber Journals. Copyright ©2025 by Dennis Barber Ltd. All rights reserved.

Table 3. Post hoc Bonferroni multiple comparisons of L^*_w (A), a^*_w (B), b^*_w (C), (D) color difference (ΔE_{diff}) of traditional (T) and glass infiltrated (G) monochrome (Mo) and multilayer [Mu, cervical (C), incisal (I)] 5Y-PSZ upon slow (S), normal (N), and fast (F) thermal tempering processes.

A. Post hoc of L^*_w as a function of material, sintering, and thermal tempering processes

Material	Mo	MuC	MuI	Sintering	T	G	Tempering	S	N	F
Mo	1	0.130	1	T	1	0.001	S	1	1	0.001
MuC		1	0.020	G		1	N		1	0.001
MuI			1				F			1

B. Post hoc of a^*_w as a function of material, sintering, and thermal tempering processes

Material	Mo	MuC	MuI	Sintering	T	G	Tempering	S	N	F
Mo	1	0.001	0.112	T	1	0.001	S	1	0.001	0.001
MuC		1	0.001	G		1	N		1	0.231
MuI			1				F			1

C. Post hoc of b^*_w as a function of material, sintering, and thermal tempering processes

Material	Mo	MuC	MuI	Sintering	T	G	Tempering	S	N	F
Mo	1	0.052	0.001	T	1	0.001	S	1	0.001	0.001
MuC		1	0.001	G		1	N		1	0.001
MuI			1				F			1

D. Post hoc of ΔE_{diff} as a function of material, sintering, and thermal tempering processes

Material	Mo	MuC	MuI	Sintering	T	G	Tempering	S	N	F
Mo	1	0.125	0.001	T	1	0.001	S	1	0.001	0.001
MuC		1	0.001	G		1	N		1	0.951
MuI			1				F			1

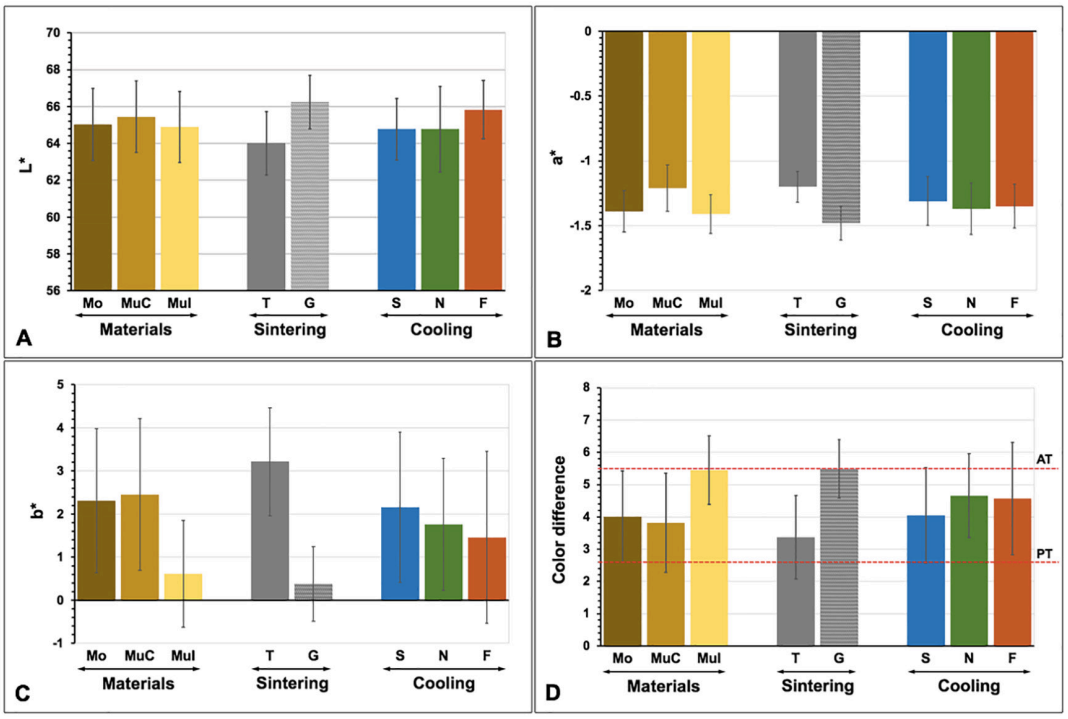

Figure 3: Influence of materials [monochrome (Mo), multilayer (Mu, C: cervical; I: incisal)], sintering techniques [traditional (T), glass infiltration (G)], and thermal tempering processes [slow (S), normal (N), fast (F)] on L* (A), a* (B), b* (C), and color difference (D) with perceptible (PT) and acceptable threshold (AT).

ejprd.org - Published by Dennis Barber Journals. Copyright ©2025 by Dennis Barber Ltd. All rights reserved.

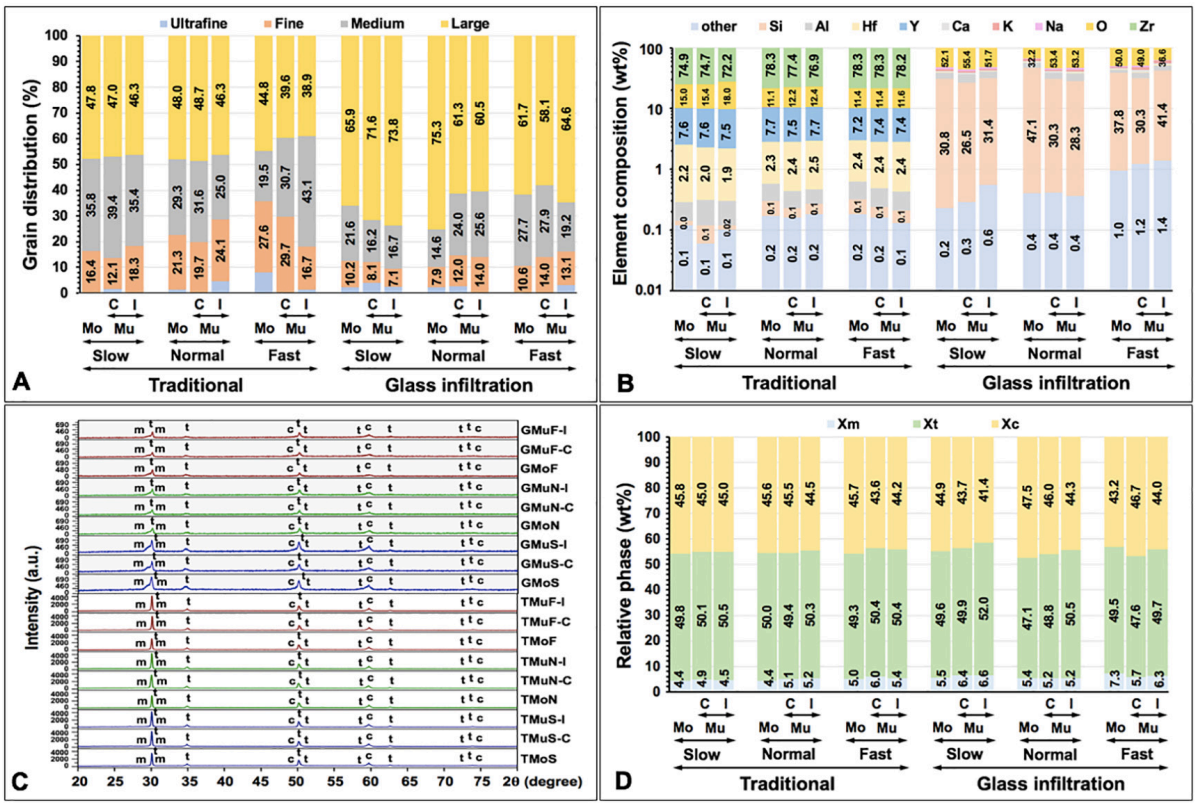

Figure 4: Grain distribution (A), elemental composition (B), x-ray diffraction angle (C), and relative phase of zirconia (D) of traditional (T) and glass infiltrated (G) monochrome (Mo) and multilayer [Mu, at cervical (C), and incisal (I) layer] 5Y-PSZ upon slow- (S), normal- (N), and fast- (F) thermal tempering processes.

(less red-yellow but more green-blue) than the C-zone of 5Y-SPZ, possibly due to differences in the addition of color pigments such as Fe (producing green) and Co (producing blue). Moreover, cerium and bismuth in higher concentrations could raise the b* value.[7] This is possibly due to differences in grain size. The grain size average of Mo was the biggest followed by MuC and MuI. The larger grain allowed more light transmission since it presented less grain boundary where the light usually scatters. Another study supported that the I-zone had less lightness than the C-zone of 5Y-PSZ.[26] However, a different study argued that higher lightness values were observed in the I-zone instead of the C-zone[27], possibly due to variations in material brand and composition. The different color additives between layers of 5Y-PSZ also affected the lightness of the materials.[28] The XRD analysis indicated that the proportion of the c-phase appeared slightly higher in Mo than in MuC and MuI. The isotropic c-phase improved material translucency by exhibiting a more uniform emission of incident light across the structure and causing less light scattering.[3]

The application of glass also had significant effects on all color parameters. An increase in L* but a decrease in a* and b* were observed in the glass infiltration group. As a result, a more white-chalky appearance and less chroma (less red-yellow but more green-blue) were observed. This color shift resulted in 5Y-PSZ having less translucency. This might be attributed to the glass infiltration powder being composed of various elements with different refractive indices, causing light scattering at the boundary between each composition. In the firing process, liquefied glass infiltrated the zirconia grain boundaries, facilitated by capillary action, leading to the formation of a glass-rich layer and a glossy surface.[15] The presence of porosity in this glass layer could generate light scattering and reduce translucence, as supported by a previous study.[19] On the other hand, another study demonstrated an equal translucence in graded zirconia compared to its non-infiltration counterpart.[16] This discrepancy between studies may arise because, in that study, they removed the excessive glass layer from the external surface before conducting optical property tests. In contrast, in our study, we examined the color parameters considering the residual glass thickness of about 60-80 µm. Regarding the microstructure, the grain size of glass-infiltrated 5Y-PSZ increased by approximately 16% compared to the non-infiltration groups. This increase could be attributed to the additional firing procedure performed for glass infiltration, which promoted grain growth and complete integration between grains and into the glass. This enlargement of grain might induce spontaneous transformation from the t- to m-phase upon cooling.[23] Such a shift typically occurs when grain sizes are above 1 µm.[23] Larger grain sizes generally result in better translucence. However, the graded zirconia, composed of different refractive indices and composition in the residual glass layer, infiltration zone, and dense zirconia, had a more significant influence on light transmission than the overall grain size.

The microstructure of zirconia is influenced by firing settings in various ways, including vacancy, crystalline phase, size and development of the grains, and density.[10,21,23,24] In this study, fast thermal tempering increased L* but decreased a* and

ejprd.org - Published by Dennis Barber Journals. Copyright ©2025 by Dennis Barber Ltd. All rights reserved.

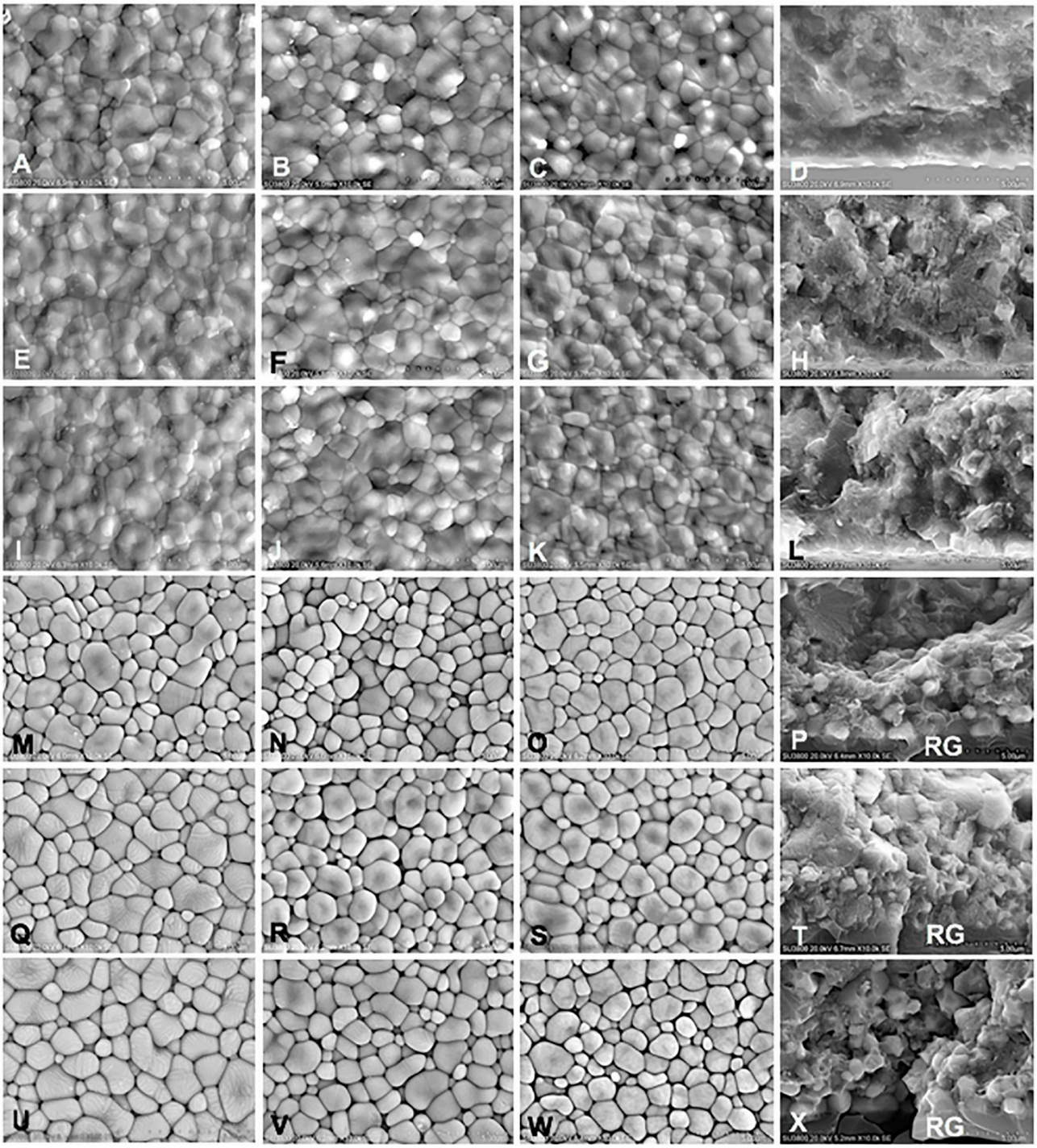

Figure 5: Scanning electron microscope photomicrographs at ×10K magnification indicated grain size and grain distribution of 5Y-PSZ traditional monochrome (A-D), multilayer [E-L: cervical (E-H), incisal (I-L)], and glass infiltrated monochrome (M-P), multilayer [Q-X: cervical (Q-T), incisal (U-X)], upon slow (A, E, M, Q, U), normal (B, F, J, N, R, V), and fast (C, G, K, O, S, W) thermal tempering processes. The micrographs of the cross-sectional surface of traditional sintered (D, H, L) and glass infiltrated (P, T, X) 5Y-PSZ, revealed a layer of residual glass (RG).

b*, significantly rendering the 5Y-PSZ a chalky white and less chromatic (less red-yellow but more green-blue). The smaller grain size produced by rapid tempering resulted in more light scattering and less light transmission at the grain boundary, contributing to the decreased translucency of the materials. The rapid tempering process could also induce defects or porosity, preventing the complete integration and tight bond of grains.[29,30] However, another study showed better translucence and larger grains in rapid cooling[23]; this difference might be attributed to the use of different materials.[31] We used 5Y-PSZ, which had a different yttria dopant, a different amount of zirconia phase, and a different effect on grain size compared to 3Y-TZP in their study. Additionally, we found that the m-phase relatively increased with an increase in the speed of thermal tempering, supported by a previous study.[23] When a material is rapidly cooled, it may experience thermal shock, leading to the formation of residual stresses that induce the microstructural conversion of zirconia from the t→m-phase.[10,23,24] The increase

ejprd.org - Published by Dennis Barber Journals. Copyright ©2025 by Dennis Barber Ltd. All rights reserved.

in the m-phase might have a more pronounced effect on birefringence among interfaces of different crystal structures. Moreover, the c-phase seemed to decline in fast tempering, which also diminished the translucency of the materials.

The assessment of the color difference value is crucial for color matching to the VITA classical shade tab, with a lower ΔE_{diff} value indicating better color matching. Among the material types, the C-zone of Mu had the lowest ΔE_{diff} value. Glass-infiltrated 5Y-PSZ exhibited a higher ΔE_{diff} value than non-infiltrated 5Y-PSZ. Regarding the thermal tempering strategy, the fast tempering produced a higher ΔE_{diff} value than others. However, the ΔE_{diff} values for different materials, glass applications, or tempering strategies remained within an AT ($\Delta E_{diff} \leq 5.5$).[14] Performing glass infiltration with a fast cooling strategy resulted in the highest ΔE_{diff} value on an incisal layer of multilayer zirconia, exceeding the acceptability limit ($\Delta E_{diff} > 5.5$).[14] According to the infiltration zone, slower tempering appeared to result in a shallower infiltration depth and thicker residual glass. This might be attributed to the limited capability of glass infiltration in porous zirconia. The porous zirconia subjected to slow-speed firing exhibited stronger grain integration with smaller and fewer gaps, which was inefficient for deep glass infiltration. However, the complete integration between the grain boundary and glass in slow tempering might have a more significant impact on enhanced translucency than the depth of infiltration.

Regarding the limitations of this study, distinguishing between the t'- and c-phases of zirconia using XRD was challenging due to their similar crystal structures and lattice parameters, resulting in strong overlapping diffraction patterns. In some cases, discrimination between the two phases can be achieved by assessing their tetragonality (c/a ratios) or utilizing alternative analytical techniques such as transmission electron microscopy (TEM) or Raman spectroscopy.[32] Therefore, it is crucial to employ multiple analytical techniques to accurately identify and quantify the different phases present in a zirconia sample. Different zirconia brands, varying glass compositions, different commercial infiltration glass, and sintering techniques, as well as exposing the specimen to different environments such as coffee, wine, or tobacco to mimic the real oral cavity environment, may yield different results, necessitating more in-depth for further investigation for color stability. Moreover, a study on the mechanical characteristics including flexural strength, fracture toughness, hardness, and roughness of 5Y-PSZ with the devised glass infiltration and tempering strategies in the artificial accelerated aging condition should be conducted to predict for strength and wear behavior of these materials in high occlusal load areas, as well as to assess long-term color stability.

Based on this recent study, the color parameters of 5Y-PSZ were influenced by the type of materials, glass infiltration, and thermal tempering process. Glass infiltration altered the color characteristics of 5Y-PSZ due to the differences in refractive indices among various compositions. The fast tempering strategy also increased lightness since it interrupted the complete integration of grains and produced smaller grains, leading to more light scattering. The application of glass and increasing the rate of thermal tempering resulted in a whiter appearance, less red-yellow, and more green-blue in 5Y-PSZ. Nevertheless, the alteration of color of Mu and Mo 5Y-PSZ upon glass infiltration, and varying thermal tempering process remained within an acceptable color difference threshold of ($\Delta E_{diff} \leq 5.5$). Hence, the color of either Mu or Mo 5Y-PSZ upon glass infiltration and varying thermal tempering was considered to be a stable and cost-effective strategy.[19-21]

CONCLUSION

Materials, glass infiltration, and tempering strategies, along with their interactions affected all color characteristics, except for the interaction of material and glass to a*, and all interactions to L*. The monochrome 5Y-PSZ had more lightness than the multilayer 5Y-PSZ, possibly due to pigment additives. Glass infiltration increased lightness as a result of the dissimilar refractive index of components. Accelerating the thermal tempering process of 5Y-PSZ resulted in increasing lightness, as it produced smaller grains and a transformation from t- to m-phase. The application of glass and increasing the rate of thermal tempering produced a whiter appearance, reduced red-yellow, and increased green-blue in 5Y-PSZ. However, the alteration of color appearance of different materials upon glass applications, and tempering strategies remained within an acceptable threshold of color appearance difference ($\Delta E_{diff} \leq 5.5$). Thus, the color appearance of either Mo or Mu 5Y-PSZ upon glass infiltration and varying tempering processes was considerably stable.

CLINICAL SIGNIFICANCE

To produce materials with enhanced optimal color appearance, it is recommended to use Mo 5Y-PSZ, combined with slow tempering, without glass infiltration. Infiltration zirconia with glass or rapid thermal tempering produced a more white-chalky and less chromatic appearance, compared to its non-infiltrated counterpart. Nevertheless, the alterations of the color appearance of either Mu or Mo 5Y-PSZ upon glass infiltration and varying tempering processes were within the acceptable threshold of color difference. Thus, sintering either Mu or Mo 5Y PSZ using glass infiltration upon varying tempering processes can be performed since color alterations were minute and considerably stable in color.

ACKNOWLEDGMENTS

The authors gratefully acknowledged the Faculty of Dentistry, Khon Kean University, Ministry of Higher Education, Science, Research and Innovation, and Royal Thai Government for providing financial support for this study. (Grant No. DTR6410/23112564).

ejprd.org - Published by Dennis Barber Journals. Copyright ©2025 by Dennis Barber Ltd. All rights reserved.

CONFLICT OF INTEREST

The authors have no conflict of interest to declare.

REFERENCES

1. Denry, I.L. and Kelly, J.R. Emerging ceramic-based materials for dentistry. *J Dent Res*. 2014; **93**:1235-1242.
2. Lughi, V. and Sergo, V. Low temperature degradation -aging of zirconia: A critical review of the relevant aspects in dentistry. *Dent Mater*. 2010; **26**:807-820.
3. Stawarczyk, B., Keul, C., Eichberger, M., Figge, D., Edelhoff, D. and Lümkemann, N. Three generations of zirconia: From veneered to monolithic. Part I. *Quintessence Int*. 2017; **48**:369-380.
4. Kulyk, V., Duriagina, Z., Kostryzhev, A., Vasyliv, B., Vavrukh, V. and Marenych, O. The effect of yttria content on microstructure, strength, and fracture behavior of yttria-stabilized zirconia. *Materials (Basel).* 2022: **15**:5212.
5. Kolakarnprasert, N., Kaizer, M.R., Kim, D.K. and Zhang, Y. New multi-layered zirconias: Composition, microstructure and translucency. *Dent Mater*. 2019; **35**:797-806.
6. Alves, M., Abreu, L., Klippel, G., Santos, C. and Strecker, K. Mechanical properties and translucency of a multi-layered zirconia with color gradient for dental applications. *Ceram Int*. 2021: **47**:301-309.
7. Shah, K., Holloway, J.A. and Denry, I.L. Effect of coloring with various metal oxides on the microstructure, color, and flexural strength of 3Y-TZP. *J Biomed Mater Res B Appl Biomater*. 2008: **87**:329-337.
8. Yu, N.K. and Park, M.G. Effect of different coloring liquids on the flexural strength of multilayered zirconia. *J Adv Prosthodont*. 2019; **11**:209-214.
9. Yan, J., Kaizer, M.R. and Zhang, Y. Load-bearing capacity of lithium disilicate and ultra-translucent zirconias. *J Mech Behav of Biomed Mater*. 2018; **88**:170-175.
10. Juntavee, N. and Attashu, S. Effect of sintering process on color parameters of nano-sized yttria partially stabilized tetragonal monolithic zirconia. *J Clin Exp Dent*. 2018; **10**:e794-e804.
11. Bona, A.A., Nogueira, A. and Pecho, O. Optical properties of CAD-CAM ceramic systems. *J Dent*. 2014; **42**:1202-1209.
12. Cho, M.S., Yu, B. and Lee Y.K. Opalescence of all-ceramic core and veneer materials. *Dent Mater*. 2009; **25**:695-702.
13. Lee, Y.K. and Yu, B. Measurement of opalescence of tooth enamel. *J Dent*. 2007; **35**:690-694.
14. Douglas, R.D., Steinhauer, T.J. and Wee A.G. Intraoral determination of the tolerance of dentists for perceptibility and acceptability of shade mismatch. *J Prosthet Dent*. 2007; **97**:200-208.
15. Zhang, Y. and Kim, J.W. Graded structures for damage resistant and aesthetic all-ceramic restorations. *Dent Mater*. 2009; **25**:781-790.
16. Mao, L., Kaizer, M.R., Zhao, M., Guo, B., Song, Y.F. and Zhang, Y. Graded ultra-translucent zirconia (5Y-PSZ) for strength and functionalities. *J Dent Res*. 2018; **97**:1222-1228.
17. Jitcharoen, J., Padture, N., Giannakopoulos, A. and Suresh, S. Hertzian-crack suppression in ceramics with elastic-modulus-graded surfaces. *J Am Ceram Soc*. 2005; **81**:2301-2308.
18. Zhang, Y., Chai, H., Lee, J.J. and Lawn, B.R. Chipping resistance of graded zirconia ceramics for dental crowns. *J Dent Res*. 2012; **91**:311-315.
19. Volpato, C.A.M., Carvalho, O..S.N., Pereira, M. and Correia Pereira da Silva, F.S. Evaluation of the color and translucency of glass-infiltrated zirconia based on the concept of functionally graded materials. *J Prosthet Dent*. 2019; **121**:547.e1-547.e7.
20. Ren, L., Janal, M. and Zhang, Y. Sliding contact fatigue of graded zirconia with external esthetic glass. *J Den Res*. 2011; **90**:1116-1121.
21. Uasuwan, P., Juntavee, N. and Juntavee, A. Optical characteristics of monochrome and Multilayer fully stabilized Zirconia upon Sintered cooling speed. *Eur J Dent*. 2014; **18**:196-204.
22. Kim, H.K. Effect of a rapid-cooling protocol on the optical and mechanical properties of dental monolithic zirconia containing 3-5 mol% Y_2O_3. *Materials (Basel)*. 2020; **13**:1923.
23. Juntavee, N. and Uasuwan, P. Influence of thermal tempering processes on color characteristics of different monolithic computer-assisted design and computer-assisted manufacturing ceramic materials. *J Clin Exp Dent*. 2019; **11**:e614-e624.
24. Juntavee, N. and Uasuwan, P. Flexural strength of different monolithic computer-assisted design and computer-assisted manufacturing ceramic materials upon different thermal tempering processes. *Eur J Dent*. 2020; **14**:566-574.
25. Sailer, I., Holderegger, C., Jung, R.E., *et al*. Clinical study of the color stability of veneering ceramics for zirconia frameworks. *Int J Prosthodont*. 2007; **20**:263-269.
26. Shirani, M., Savabi, O., Mosharraf, R., Akhavankhaleghi, M., Hebibkhodaei, M. and Isler, S. Comparison of translucency and opalescence among different dental monolithic ceramics. *J Prosthet Dent*. 2021; **126**: 446.e1-446.e6.
27. Cho, M.H. and Seol, H.J. Optical properties, microstructure, and phase fraction of multi-layered monolithic zirconia with and without yttria-gradient. *Materials (Basel)*. 2022; **16**: 41.
28. Pekkan, G., Pekkan, K., Bayindir, B., Özcan, M. and Karasu, B. Factors affecting the translucency of monolithic zirconia ceramics: A review from a materials science perspective. *Dent Mater J*. 2020; **39**:1-8.
29. Vichi, A., Sedda, M., Fabian Fonzar, R., Carrabba, M. and Ferrari, M. Comparison of contrast ratio, translucency parameter, and flexural strength of traditional and "augmented translucency" zirconia for CEREC CAD/CAM system. *J Esthet Restor Dent*. 2016; **28**:S32-S39.
30. Uasuwan, P., Juntavee, N. and Juntavee, A. Flexural strength of high yttrium oxide-doped monochrome and multilayered fully stabilized zirconia upon various sintered cooling rates. *J Prosthodont*. 2023; **32**:e118-e128.
31. Shetty, M., Jain, S., Wankhede, T. M., *et al*. An *in vitro* study to evaluate the effect of artificial aging on translucency, contrast ratio, and color of zirconia dental ceramic at different sintering levels. *Coatings*. 2020; **12**:642.
32. Gibson, I.R. and Irvine, J.T.S. Qualitative X-ray diffraction analysis of metastable tetragonal (t') zirconia. *J Am Ceram Soc*. 2001; **84**:615-618.

ejprd.org - Published by Dennis Barber Journals. Copyright ©2025 by Dennis Barber Ltd. All rights reserved.